Brigham Young University
BYU ScholarsArchive

Theses and Dissertations

2012-07-31

Design and Testing of a Biological Microelectromechanical System for the Injection of Thousands of Cells Simultaneously

Gregory Herlin Teichert
Brigham Young University - Provo

Follow this and additional works at: https://scholarsarchive.byu.edu/etd

 Part of the Mechanical Engineering Commons

BYU ScholarsArchive Citation

Teichert, Gregory Herlin, "Design and Testing of a Biological Microelectromechanical System for the Injection of Thousands of Cells Simultaneously" (2012). *Theses and Dissertations*. 3366.
https://scholarsarchive.byu.edu/etd/3366

This Thesis is brought to you for free and open access by BYU ScholarsArchive. It has been accepted for inclusion in Theses and Dissertations by an authorized administrator of BYU ScholarsArchive. For more information, please contact scholarsarchive@byu.edu, ellen_amatangelo@byu.edu.

Design and Testing of a Biological Microelectromechanical System for the Injection of Thousands of Cells Simultaneously

Gregory H. Teichert

A thesis submitted to the faculty of
Brigham Young University
in partial fulfillment of the requirements for the degree of

Master of Science

Brian D. Jensen, Chair
Larry L. Howell
Sandra H. Burnett

Department of Mechanical Engineering

Brigham Young University

December 2012

Copyright © 2012 Gregory H. Teichert

All Rights Reserved

ABSTRACT

Design and Testing of a Biological Microelectromechanical System for the Injection of Thousands of Cells Simultaneously

Gregory H. Teichert
Department of Mechanical Engineering, BYU
Master of Science

The ability to inject DNA and other foreign particles into cells, both germ cells (e.g. to produce transgenic animals) and somatic cells (e.g. for gene therapy), is a powerful tool in genetic research. Nanoinjection is a method of DNA delivery that combines mechanical and electrical methods. It has proven to have higher cell viability than traditional microinjection, resulting in higher integration per injected embryo.

The nanoinjection process can be performed on thousands of cells simultaneously using an array of microneedles that is inserted into a monolayer of cells. This thesis describes the needle array design requirements and the fabrication process used to meet them. The process uses unpassivated and passivated deep reactive ion etching (DRIE) to create needles with a constant diameter shaft and a pointed tip. The needle diameter and height are about 1 μm and 8 μm, respectively. A buckling analysis and physical testing show that the needles can withstand the force required to penetrate the cells.

The chip is attached to a plastic suspension with a counter electrode and electrical connections to a voltage source. The suspension's motion is defined by two compliant orthoplanar springs that have been vertically and rotationally offset for added stability. The base of the suspension is designed to exactly fit in the bottom of a cell culture dish, where the needle array can be pushed into the cell monolayer.

Injection protocol was created and followed to perform tests with needle insertion only, voltage application only, and the full nanoinjection process. The average cell viability for the full injection process was 98.2% compared to an average control viability of 99.5%. Zero volt injections with a high concentration of propidium iodide, a cell impermeable dye with two positive charges, resulted in dye uptake from diffusion, proving that the needles are penetrating the cells. Tests comparing injections with and without voltage had high variability in dye uptake. Therefore, glass cover slips were placed in the culture dishes to provide more consistent injection conditions. This reduced variation in zero voltage tests. It is recommended that this procedure be followed for performing injections with voltage.

Keywords: MEMS, microinjection, nanoinjection, microneedles, DRIE, cell culture

ACKNOWLEDGMENTS

The work accomplished and results presented in this thesis would not have been possible without the help and support of my family, my fellow students, and the faculty and staff at Brigham Young University. I acknowledge the funding support by the National Science Foundation Graduate Research Fellowship under Grant No. DGE-0750759. I particularly thank my graduate advisor and committee members, Dr. Jensen, Dr. Howell, and Dr. Burnett, as well as Brother Barben of the RIC Facility, for the opportunities and support they have given me.

I also thank the students of the Compliant Mechanisms Research group, especially Steven Brewer, Melanie Easter, and Nathan Toone, who have helped with the needle fabrication and cell culture, as well as giving sound advice throughout this project.

Most of all, I thank my wife, Michelle, and son, Hyrum, whose love motivates and encourages me to do my best, and God, for the inspiration, guidance, and purpose He generously gives.

TABLE OF CONTENTS

LIST OF TABLES

LIST OF FIGURES

CHAPTER 1. INTRODUCTION

The ability to inject DNA and other foreign particles into cells, both germ cells (e.g. to produce transgenic animals) and somatic cells (e.g. for gene therapy), is a powerful tool in genetic research. Several current methods of DNA delivery are analyzed by [1, 2] including viral, mechanical, electrical, and chemical methods. Viral methods are reported as being the most effective, but they present several challenges, including toxicity, limited DNA carrying capacity, and high cost. Microinjection is also reported as being relatively effective and having low toxicity, but it is laborious and time intensive since cells are injected one at a time. Nanoinjection uses a mechanical method similar to microinjection, but it also incorporates electrical methods in the injection process [3–9]. While the current nanoinjection system, like microinjection, is limited to injecting cells individually, it has potential to inject multiple cells at the same time using an array of microneedles. This thesis presents a microneedle array fabrication method, injection system setup, and injection protocol that provide a basis for the adaptation of nanoinjection to a simultaneous multi-cell injection system.

1.1 Nanoinjection

The nanoinjection process uses a solid needle, termed a lance, and a counter electrode (see Figure 1.1). Both are placed in a solution with the cells to be injected. The lance is electrically charged with a positive charge, and DNA is added to the solution. The DNA, which has a double negative surface charge, accumulates on the lance. The lance is inserted into one of the pronuclei of the cell, the charge is reversed to release the DNA, and the lance is removed. The process can be modified using electroporation to introduce the DNA into one of the pronuclei. The lance would be used as before to transfer the DNA into the cytoplasm. A high voltage would then be used to both electroporate the pronuclei and repel the DNA from the lance and into at least one of the pronuclei.

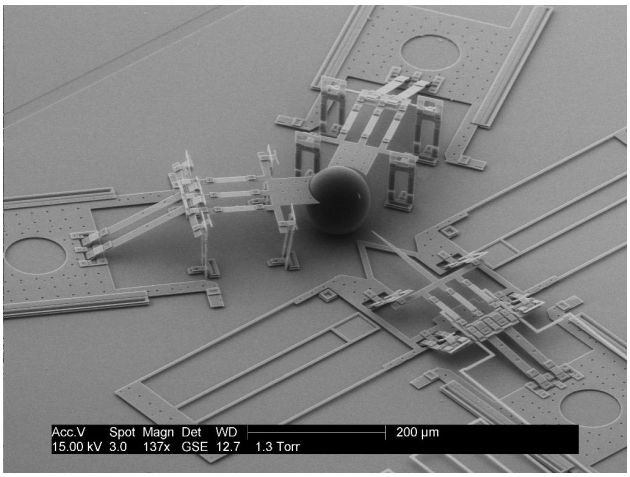

Figure 1.1: SEM (scanning electron micrograph) of the on-chip MEMS nanoinjector.

Side-by-side studies were done with microinjection and nanoinjection [9]. Nanoinjection resulted in 6.2% integration per injected embryo while microinjection resulted in 1.6%. This is largely due to the higher levels of cell viability from nanoinjection. 77.6% of nanoinjected embryos proceeded to the two-cell stage compared to 54.7% of microinjected embryos. The increase in viability is likely due to the smaller cross-section of the nanoinjection lance (0.06 μm^2) compared to a microinjection needle (0.78 μm^2). Furthermore, nanoinjection inserts the DNA without injecting any extracellular fluid, unlike microinjection.

1.2 Microneedle Arrays

The nanoinjection system is currently limited to the injection of individual cells on the order of 80 μm in diameter. Using microneedle arrays, it will be possible to inject multiple cells simultaneously, including smaller somatic cells. The majority of microneedle arrays are on the order of 100 μm tall [10–15]. McAllister et al. fabricated an array of solid microneedles to show the ability to deliver foreign particles into thousands of cells simultaneously [16]. The array included 160,000 needles spaced 25 μm apart with a base diameter of 15 μm, a tip diameter less than 1 μm, and a height of 25 μm (see Figure 1.2(b)). The array was inserted into a monolayer of prostate cancer cells (approximately 25 μm in diameter) that had been bathed in a solution containing a fluorescent molecule. After the needles were retracted from the cells, the fluorescent

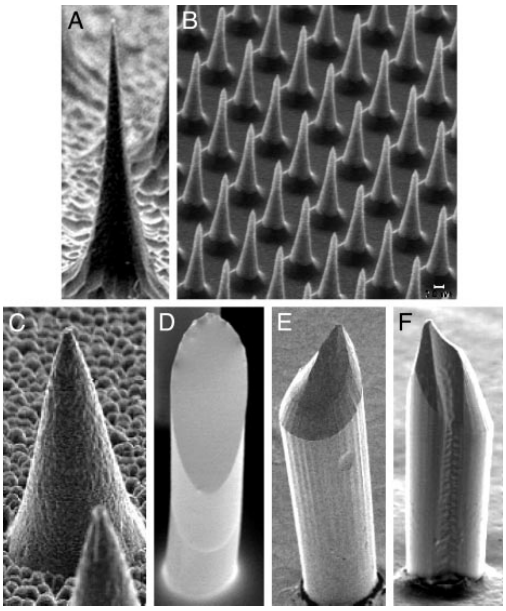

Figure 1.2: SEMs (scanning electron micrographs) of microneedles fabricated of silicon, polymer, and metal using several different methods [16].

molecule had been delivered to about 85% of the cells. A viability stain showed that about 90% of the cells were viable.

Microneedle arrays have also been used for electroporation [14, 17]. Choi et al. developed an electrically functional microneedle array for eventual use in the electroporation of epidermal cells to increase transfection of DNA vaccines. The purpose of these microneedles is not to individually penetrate the cells. The microneedles are first used to help the vaccine penetrate the stratum corneum (a layer of dead tissue that protects the living skin cells). They are then used as the electrodes for electroporation. The small size and close spacing of the microneedles require a relatively low voltage to achieve the high electric field necessary for electroporation. Many methods have been developed for fabricating microneedles. McAllister, et al. report several fabrication methods that fall into two categories [16] (see Figure 1.2). The first category involves directly etching the microneedles from a substrate, typically silicon. The second category involves creating a micromold, usually by etching, and then filling the mold with metal or polymer. Hollow microneedles were formed by using solid microneedles as the micromold. A thin layer of material was coated on the solid microneedle, after which the solid microneedle was removed to leave a hollow core. Another fabrication method that falls in the etching category is shown by Gassend

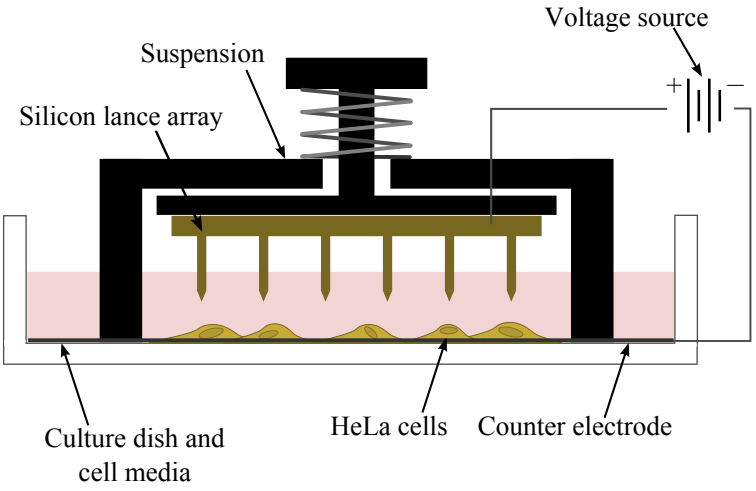

Figure 1.3: This schematic describes the layout of the injection system. The needle array chip is attached to the chip suspension and connected to a voltage source. The suspension is lowered into a culture dish of cells for injection.

et al. in [18]. This process involves both unpassivated and passivated deep reactive ion etching (DRIE) to produce a needle with a shaft of constant diameter except at the tip, where the needle tapers to a sharp point.

1.3 Research Objectives and Thesis Outline

This research project met three main objectives:

1. Fabricate needle arrays that are able to penetrate a cell monolayer without causing significant cell death.

2. Design an appropriate system for performing injections.

3. Develop a protocol for the lance array injection system and test with a dye.

Chapter two specifies the needle array design requirements and the fabrication method used to meet them. Needle arrays were fabricated from single-crystal silicon using DRIE, producing 2 x 2 cm chips with approximately 4 million needles. The needles are an average of 1 μm in diameter and 8 μm tall with 10 μm center-to-center spacing. Various studies were done of the etches used in the process to gain further control over the final needle geometry. A buckling analysis verifies the feasibility of the needle dimensions specified in the design requirements.

The third chapter describes the injection system and the necessary design constraints. Three suspensions were designed using a compliant orthoplanar spring to allow vertical displacements but minimize all other deflections. The third chip suspension incorporates an electrical connection to the chip and counter electrode, allowing it to be used with the full nanoinjection process.

Chapter four describes the injection protocol developed for testing with HeLa 229 cells (see Figure 1.3). Cell viability is reported for tests done with needle insertion only, voltage only, and the full nanoinjection protocol. Propidium iodide, a membrane impermeable dye with two positive charges per molecule, was used in injections with and without voltage. It was shown through diffusion of the dye into the cells that the needles are piercing the cell membrane. Performing injections on glass cover slips may provide a more consistent injection environment.

CHAPTER 2. NEEDLE ARRAY FABRICATION

This chapter presents the design and fabrication of the needle array, studies concerning the etches used in the fabrication process, and a buckling analysis of the needles.

There were at least five design requirements for the needle array:

1. The needle array must be made of an electrically conductive material for the nanoinjection process to apply.

2. The needles need to be spaced in such a way to inject every cell in the culture. Round HeLa cells are about 15 μm in diameter when adhered [19]. However, HeLa cells generally stretch when they adhere to the culture dish, often reaching over 50 μm in length with a 10 μm width (see Figure 2.1).

3. The needles should have a pointed tip to facilitate piercing of the cell.

4. The needles should be taller than the HeLa cells are thick to avoid additional stress due to the substrate pressing against the cells. HeLa cells are usually about 4 μm thick, although they can be more than 8 μm thick [20, 21].

5. The needle shaft should be narrow (approximately 1 μm diameter) to minimize cell death.

The following fabrication process is designed to meet each of these requirements.

2.1 Fabrication Process

The needle array fabrication process is based on the process reported by Gassend, et al. in [18], although certain steps and parameters have been adapted for the current application. The specific settings used in the DRIE steps can be found in Appendix A. The needle array is fabricated

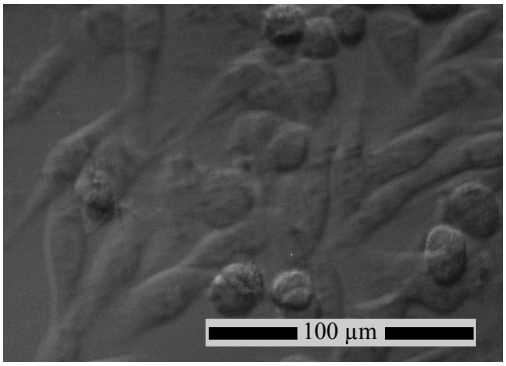

Figure 2.1: This optical micrograph shows both round and stretched HeLa cells that have adhered to a cell culture dish.

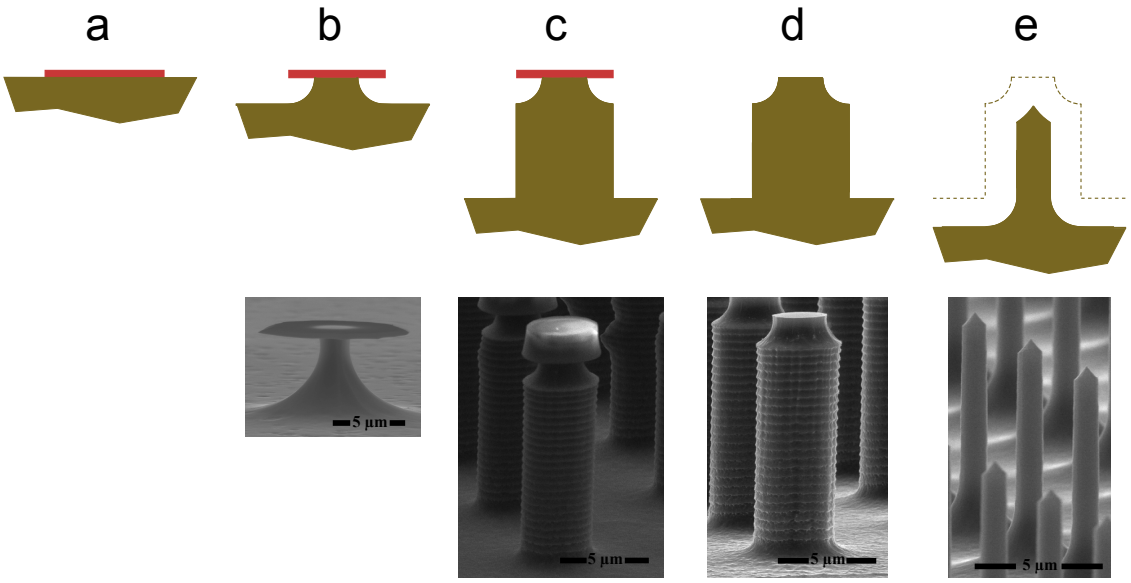

Figure 2.2: This schematic shows a sideview of the fabrication process. (a) A photoresist disc is used as a mask during (b) the first unpassivated DRIE (deep reactive ion etching) step and the (c) passivated DRIE step. (d) The photoresist mask is removed for (e) the final unpassivated DRIE step.

from single-crystal silicon in order to be electrically conductive and fulfill the first design requirement. This also takes advantage of the well established silicon etching techniques. The processing steps are as follows:

1. An array of AZ3330 positive photoresist discs is patterned onto the wafer using photolithography. These photoresist circles are used as the mask layer in the process (see Figure 2.2(a)). They have a diameter of about 5 μm and are spaced 10 μm from center to center. This

spacing ensures that each HeLa cell will be pierced at least once, according to the second design requirement. Because of variation in the photolithography, the diameter of the circles are measured in order to determine the necessary time for the final unpassivated DRIE (deep reactive ion etching) step.

2. The wafer is diced into 2 x 2 cm chips. Each chip undergoes an unpassivated DRIE step for 30 seconds to undercut the photoresist discs. This undercut will eventually form the tip of the needles described in requirement three (Figure 2.2(b)). The etch is performed with a sulfur hexafluoride plasma.

3. A passivated DRIE step is then performed to create the shaft of the needle (Figure 2.2(c)), using a 3 minute Bosch etch. This produces needles that are usually 8 μm tall, according to the fourth requirement. Needle height can be controlled completely by this step, therefore the etch time can be increased if the strain of cells used in testing is thicker than the average value of 4 μm.

4. The photoresist masks are removed with acetone (Figure 2.2(d)), and the passivation layer left by the Bosch etch is removed with a 2 minute oxygen plasma [22]. The oxygen plasma leaves a coating of silicon dioxide, which is removed by a 30 second hydrofluoric acid etch.

5. A final sulfur hexafluoride unpassivated DRIE step of about 35 seconds reduces the diameter of the shaft to the desired size and creates a tip at the end of the shaft (Figure 2.2(e)). The needles are usually between 0.5 and 1 μm in diameter (Figure 2.3(a)), satisfying design requirement five. This etch step is primarily responsible for the needle diameter and can be adjusted if a different diameter is desired.

6. If an insulative layer covering the floor layer but leaving the needles exposed is desired, a small amount of photoresist can be spun onto the chip and hard baked (see Figure 2.3(b)).

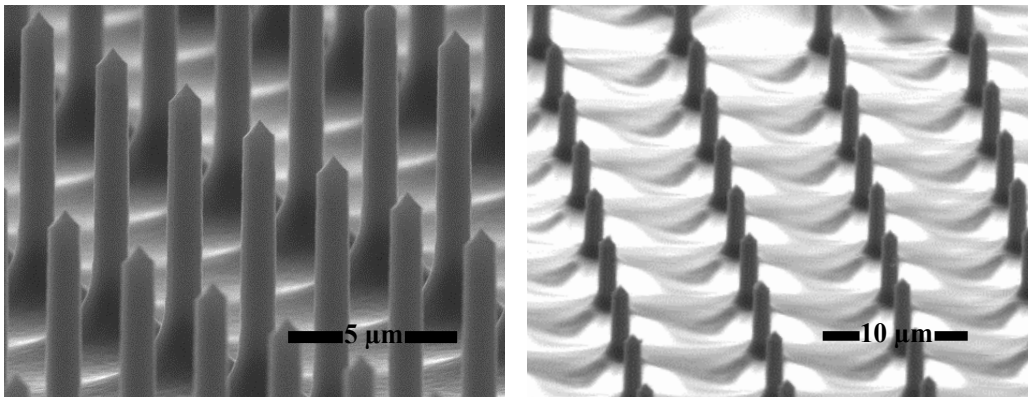

(a) Array of silicon needles (b) Photoresist insulative layer

Figure 2.3: (a) The silicon needles are usually between 0.5 and 1 μm in diameter and 8 μm long with 10 μm spacing. (b) Photoresist can be used to create an insulative floor layer.

2.2 Etch Studies

Four etch studies are reported here. These were done to understand the effect of the etch parameters on the final needle geometry. This led to greater control over the fabrication process and allowed the needle design requirements to be met.

The first two studies involve two methods of passivated DRIE: continuously passivated DRIE and the Bosch etch. The passivated DRIE step is used to produce vertical sidewalls, but small changes in the etch parameters can affect the angle of the sidewall. These two studies explore and report on the etch parameters that affect sidewall angle. The needles should have no taper or only a slightly positive taper to minimize the cross-sectional area and the stress in the needles.

The third study looks at the sensitivity of the needle geometry to the two unpassivated DRIE steps. Both steps affect the needle tip, but only the final etch affects the needle diameter. The photolithography process leaves some variation in the photoresist mask diameter, which changes the necessary final etch time. Knowing how much each etch affects the needle geometry allows the user to know how to adjust the etches. For example, if the needle geometry is very sensitive to both unpassivated etch steps, then adjusting the final etch time will also require an adjustment to the first etch. This study shows which parameters to change and how they affect the needle.

The needle fabrication method reported by Gassend, et al. [18] leaves the etch mask on the needles for the entire process. Hanein et al. [12] remove the mask layer before producing the tip

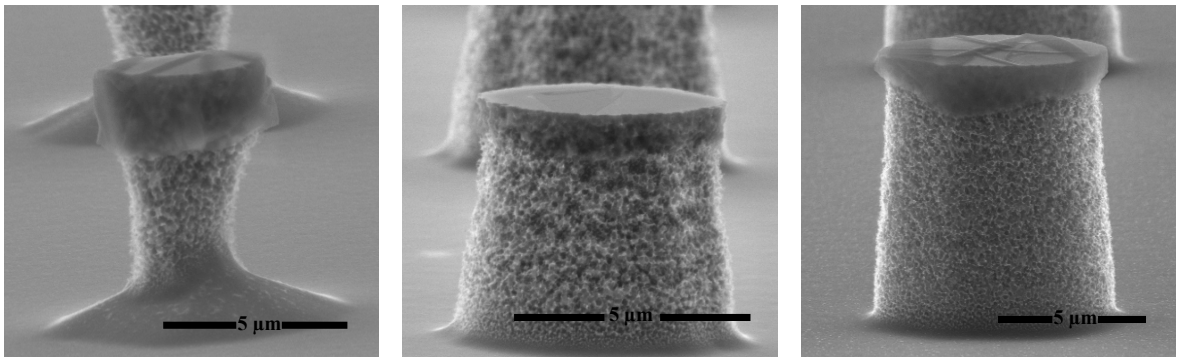

(a) 38 sccm oxygen (b) 40 sccm oxygen (c) 42 sccm oxygen

Figure 2.4: Decreasing the amount of oxygen from 40 sccm to 38 sccm caused a noticeable negative taper. However, increasing the oxygen from 40 to 42 sccm had no significant effect on taper. The difference in column height was due to different etch times.

on the needles in their fabrication process. The fourth study in this section shows the effects of each method in this fabrication process.

2.2.1 Continuously Passivated DRIE Step

A passivated DRIE step can be achieved in DRIE by combining sulfur tetrafluoride (SF_6) and oxygen (O_2) in the plasma etch. This combination has been studied in RIE (reactive ion etching), and the method of finding the combination that results in vertical sidewalls is call the black silicon method [23,24]. These studies have shown that decreasing the O_2 to SF_6 ratio creates a more negative taper. Increasing the ratio makes the taper more positive, but the effect diminishes as the amount of oxygen increases. This was also demonstrated using DRIE (see Figure 2.4). However, this combination of gases produced porous, uneven sidewalls when using DRIE, whereas the sidewalls are reported to be smooth when using RIE [23, 25]. The Bosch method produces nonporous, even sidewalls, so it was chosen for the fabrication process.

2.2.2 Bosch Etch

The Bosch etch creates a passivated DRIE step by alternating between an unpassivated DRIE step and the deposition of a passivation layer. Changing the length of the etch and deposition steps affect the taper of the sidewall. In order to minimize any negative taper, a study was done

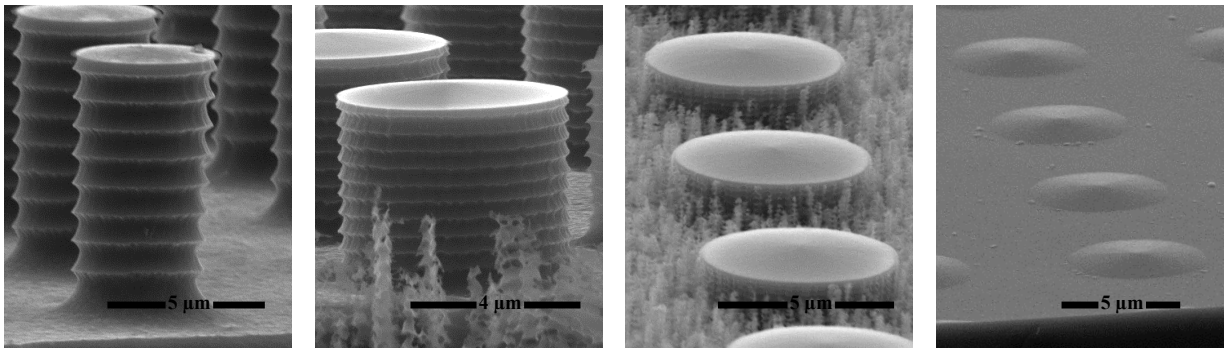

(a) 8.0 sec etch step (b) 5.0 sec etch step (c) 4.0 sec etch step (d) 3.0 sec etch step

Figure 2.5: Decreasing the etch step in the Bosch etch decreases the negative sidewall taper, as shown in (a) and (b). It can also lead to (c) silicon "grass" or (d) eventually halt etching.

to find the relationship between the etch time, passivation time, and the sidewall taper. The length of the passivation step was kept at 5.0 seconds and the total length of the Bosch etch was held constant, but the length of the etch step was changed. The results are shown in Table 2.1. The 5.0 second etch time produced the best results with a taper of 0°. It was noted that the height of the columns also decreased as the etch step was decreased. Figure 2.5 shows the results of 8.0, 5.0, 4.0, and 3.0 second etch periods. With a 4.0 second etch step and to a lesser degree with the 5.0 second etch step, silicon "grass" was produced around the columns. This is due to the positive taper produced by this etch recipe. Dust, photoresist, or other small particles on the chip act as small masks. With a negative taper these are quickly undercut, and their effect is not seen. With a positive taper, however, these particles produce slender columns whose cross section increases with the etch depth. The 3.0 second etch step was not able to etch through the passivation layer left by the 5.0 second passivation step.

Table 2.1: The Bosch etch was modified by reducing the etch step time to understand the effect on sidewall taper.

Etch Time (s)	Top Diameter (μm)	Bottom Dia. (μm)	Height (μm)	Taper
8.0	4.58	4.15	7.92	$-1.55°$
7.5	4.78	4.52	7.99	$-0.93°$
7.0	4.57	4.36	7.11	$-0.84°$
6.0	4.74	4.69	6.23	$-0.23°$
5.0	5.40	5.40	4.11	0°

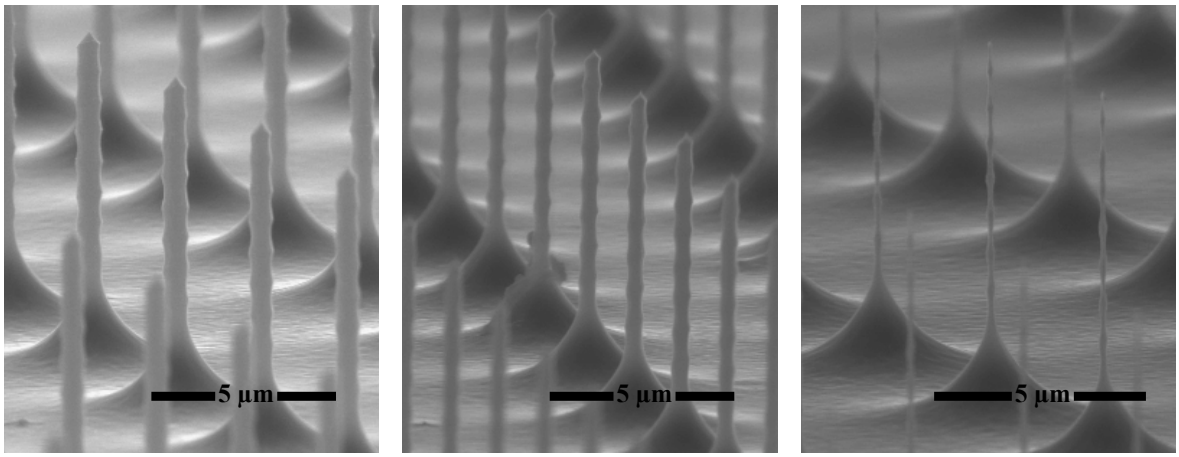

(a) Baseline etch times (b) 1st etch increased by 1 second (c) 2nd etch increased by 1 second

Figure 2.6: These SEMs show that the final needle geometry is not as sensitive to the first unpassivated DRIE step as it is to the second unpassivated DRIE step.

2.2.3 1st and 2nd Unpassivated DRIE Steps

A brief study was done to show the effect of the first and second unpassivated DRIE steps. A baseline recipe was chosen that produced needles of the proper geometry with a first unpassivated DRIE step of 20 seconds and a second unpassivated DRIE step of 18 seconds (Figure 2.6(a)). Another chip was fabricated with the first unpassivated DRIE step increased to 21 seconds and the second unpassivated DRIE step kept at 18 seconds (Figure 2.6(b)). A third chip kept the first unpassivated DRIE step at 20 seconds and increased the second unpassivated DRIE step to 19 seconds (Figure 2.6(c)). It is seen that the change in the first unpassivated DRIE step made little difference in the needle geometry, but the change in the second unpassivated DRIE step created a significant decrease in the needle diameter. Therefore, any changes in the photoresist mask size should be compensated by making small changes in the final unpassivated DRIE step.

2.2.4 Mask Removal Before and After the Second Unpassivated DRIE Step

The mask can be removed either before or after the second unpassivated DRIE step. Removing the mask before the final unpassivated DRIE step produces the tip in Figure2.7(a) uniformly across the chip. If the unpassivated DRIE step were a true isotropic etch, removing the mask after all DRIE steps would produce a sharper tip (see Figure 2.7(b)). However, since the

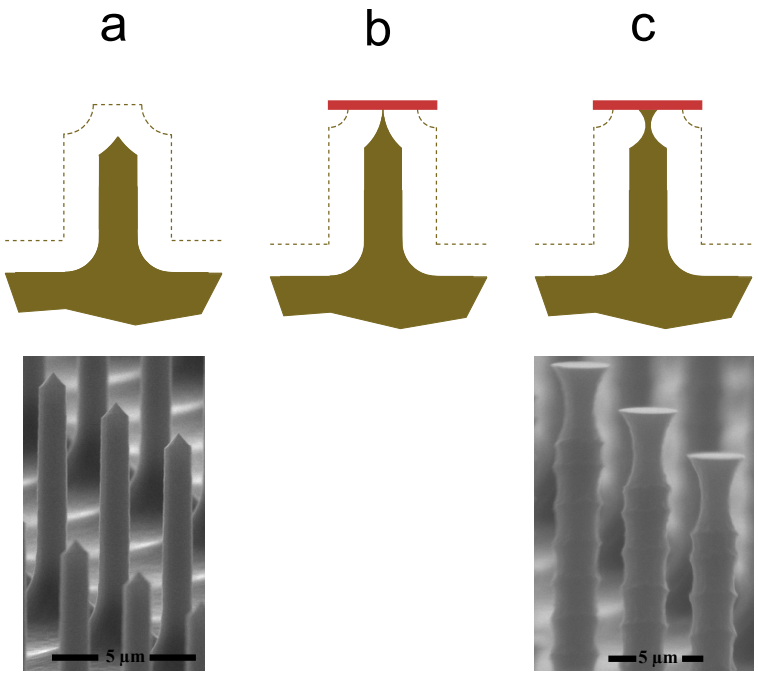

Figure 2.7: (a) Tip resulting from mask removal before the final unpassivated DRIE step, (b) tip from mask removal after an ideal isotropic etch, and (c) tip resulting from mask removal after the final unpassivated DRIE step.

unpassivated DRIE step has a slight bias towards the substrate, it produces the tip shown in Figure 2.7(c). Therefore, removing the mask before the final unpassivated DRIE etch step produces the better tip using the current etch methods. However, if a sharper tip is needed, the mask should remain for the second unpassivated etch step and a purely isotropic etch should be used.

2.3 Buckling Analysis

A buckling analysis was performed to ensure that the needle dimensions specified in the design requirements are feasible. The equations used in this section are reported in [26]. Slender columns in axial compression will fail either in compression or in buckling depending the column geometry and end conditions. The slenderness ratio S_r is used to determine which failure mode

will occur. The slenderness ratio is found using the following equations:

$$S_r = \frac{l_{eff}}{k} \tag{2.1}$$

$$k = \sqrt{\frac{I}{A}} \tag{2.2}$$

where l_{eff} is the effective length of the column based on the actual length and the end conditions, I is the area moment of inertia of the column's cross section, and A is the cross sectional area. For a circular cross section, the equation reduces to

$$S_r = \frac{2l_{eff}}{r} \tag{2.3}$$

where r is the radius of the cross section.

The needles in the array undergo a fixed-free end condition during the injection process, resulting in an effective length of $2l$, or twice the actual length of the column. The slenderness ratio then becomes

$$S_r = \frac{4l}{r} \tag{2.4}$$

If the slenderness ratio is greater than about 10, then the column will fail in buckling. The geometry of the needles is not always constant from chip to chip. However, the largest possible radius and shortest possible length can be used to find the minimum possible slenderness ratio for the needles. Given a maximum radius of 0.75 μm and a minimum length of 5 μm, the resulting slenderness ratio is 26.7. Therefore, the needles will fail in buckling when the critical load P_{cr} is applied.

The value $(S_r)_D$ is used to determine P_{cr}. It is found using

$$(S_r)_D = \pi\sqrt{\frac{2E}{S_{yc}}} \tag{2.5}$$

where E is the modulus of elasticity and S_{yc} is the yield strength in compression. If $(S_r)_D < S_r$ the following equation is used to find the theoretical P_{cr}

$$P_{cr} = \frac{\pi^2 AE}{S_r^2} \tag{2.6}$$

The modulus of elasticity of single-crystal silicon is 130 GPa for the orientation of the needles, and the average fracture strength is about 4 GPa [27]. This gives a value of $(S_r)_D$ equal to 25.3, which is less than the minimum slenderness ratio of 26.7. The maximum slenderness ratio is used to find the minimum critical load. Using a minimum radius of 0.2 μm and a maximum length of 10 μm gives a maximum slenderness ratio of 200 and a minimum critical load of 4.0 μN. The force needed to penetrate a human epidermal melanocyte is less than 2 nN [28]. It can be assumed that HeLa cells would require a penetration force of the same order of magnitude; therefore these needles should easily penetrate HeLa cells without buckling.

2.4 Conclusion

Five design requirements were specified in this chapter for the needle array to be used in the multi-cell nanoinjection process. A fabrication process was presented that produces needles that meet the design requirements. The etches used in the fabrication process were studied to better understand how the etch parameters should be adjusted to create the desired needle geometry. The sidewall taper of two methods of passivated DRIE were studied. The appropriate parameter values were found to produce little or no taper. However, the Bosch method proved to produce more even and consistent sidewalls and was chosen for the fabrication process. A study of the two unpassivated etch steps showed that the process is more sensitive to final unpassivated etch step than to the first. This means that the final etch can be adjusted for changes in the photoresist mask size without needing to adjust the first unpassivated etch to maintain a sharp tip on the needle. The fourth study showed that a better tip is produced using the described etch steps when the mask is removed before the final etch. The buckling analysis showed that the needle dimensions specified in the design requirements are feasible.

CHAPTER 3. INJECTION SYSTEM DESIGN AND FABRICATION

The injection system design has specific design objectives and constraints, as listed here:

1. Allow controlled insertion of the needles into the cell monolayer by allowing vertical displacement of the needle array and minimizing all other linear and rotational displacements.
2. Incorporate the needle array and a counterelectrode, with electrical connections to both.
3. Interface easily with the cell culture dish, which has a diameter of 34.80 mm and a depth of 17.4 mm.
4. Conform to fabrication constraints, such as minimum feature size, etc.

To meet the first design objective, the injection system is based around a suspension utilizing a compliant orthoplanar spring. The equations used in orthoplanar spring design are presented in the first section of this chapter. Three orthoplanar spring suspension designs are discussed in the following section, along with their implementation of the design objectives and constraints.

3.1 Orthoplanar Spring Design

The compliant orthoplanar spring consists of a movable platform attached to the base by multiple legs [29, 30] (see Figure 3.1). Each leg is made of two fixed-guided flexible segments in series. This configuration allows large displacements of the platform without relative rotation of the platform with respect to the base. The orthoplanar spring can be analyzed for large deflections using the pseudo-rigid-body model (PRBM), which replaces flexible segments with rigid body links, revolute joints, and torsional springs.

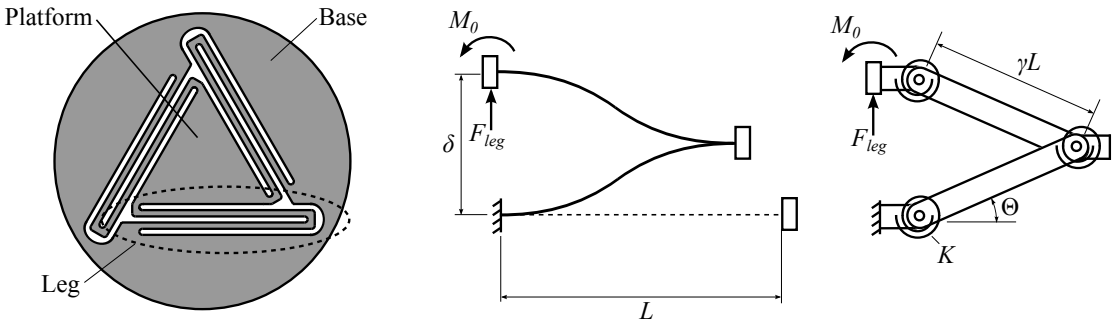

Example of a three-legged orthoplanar spring

Side-view schematic of a single leg of an orthoplanar spring

PRBM of a single leg of an orthoplanar spring

Figure 3.1: These line diagrams demonstrate the layout, motion, and modeling of an orthoplanar spring.

For a given total deflection δ, the force per leg F_{leg} and total required force F_{tot} can calculated with the following equations

$$F_{leg} = \frac{4K_\Theta EI\Theta}{L^2\cos\Theta} \tag{3.1}$$

$$F_{tot} = sF_{leg} \tag{3.2}$$

$$\Theta = \arcsin\frac{\delta}{2\gamma L} \tag{3.3}$$

where K_Θ is the stiffness coefficient (usually $K_\Theta \approx 2.65$), L is the length of each flexible segment, E is the Young's modulus, I is the area moment of inertia, Θ is the angular displacement of the PRBM, s is the number of legs, and γ is the characteristic radius factor (usually $\gamma \approx 0.85$).

The principal stresses σ_A and σ_B can also be calculated from the normal stress σ_x and the shear stress τ_{xy}, where

$$\sigma_x = \frac{K_\Theta Eh(1-\gamma(1-\cos\Theta))\Theta}{L\cos\Theta} \tag{3.4}$$

$$\tau_{xy} = \frac{K_\Theta C_T Eeh\Theta}{L^2\cos\Theta} \tag{3.5}$$

$$\sigma_A, \sigma_B = \frac{\sigma_x}{2} \pm \sqrt{\left(\frac{\sigma_x}{2}\right)^2 + \tau_{xy}^2} \tag{3.6}$$

where h is the out-of-plane thickness of the flexible segments, e is the offset from the center of one flexible segment in a leg to the other, and C_T is a constant used for calculating the shear stress for a given rectangular cross section.

For a ductile material, the safety factor SF is calculated from the equation

$$SF = \frac{S_y}{\sigma_A - \sigma_B} \tag{3.7}$$

where S_y is the yield strength of the material.

The safety factor can also be calculated for a brittle material using

$$SF = \frac{S_{ut} S_{uc}}{S_{uc}\sigma_A - S_{ut}\sigma_B} \tag{3.8}$$

where S_{ut} is the ultimate tensile strength and S_{uc} is the ultimate compressive strength.

3.2 Suspension Designs

Three suspension designs were developed for use with the needle array. The first incorporated the orthoplanar spring as part of the silicon chip. The second design used an external orthoplanar spring made of ABS plastic to which the chip was taped. The third design used two offset orthoplanar springs for added stability, and it included electrical connections and a counter-electrode for use with the full nanoinjection process. This third design is the only one to fully meet the design requirements.

3.2.1 Silicon Orthoplanar Suspension

The first suspension design included the orthoplanar spring as part of the silicon chip. Silicon dioxide is used as the mask layer for the needles, and a thick photoresist is spun onto the wafer after the oxide mask layer has been defined. The orthoplanar spring design is patterned in the photoresist and is etched with a Bosch etch. A backside etch is used to thin the wafer to the desired thickness. The needle fabrication can be continued as described previously. It is then placed on a chip holder that allows the desired displacement. The orthoplanar spring designed used the parameters used in Table 3.1 (see Figure 3.2). Since the beam dimensions are on the order

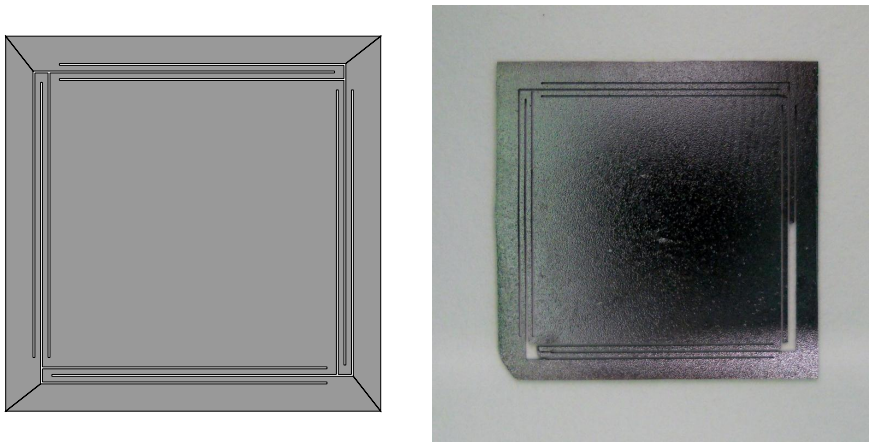

(a) Orthoplanar spring line diagram (b) Silicon orthoplanar spring

Figure 3.2: A four-legged orthoplanar spring can be incorporated into the lance array chip to serve as the suspension.

of millimeters, lower values used for the ultimate tensile and compressive strengths of polysilicon were used in the analysis of the spring [29, 31]. These parameters produced a safety factor of 2.47 for a displacement of 1 mm.

It was found that a single orthoplanar spring is effective at eliminating lateral deflections and rotations about the vertical axis. However, it did not effectively restrain rotations about the horizontal axis. Also, although this design combines the needle array and suspension, it fails to incorporate electrical connections or a counterelectrode specified in the second design constraint. The orthoplanar spring dimensions do allow it to fit within a 2 x 2 cm silicon chip, which fits within the culture dish and meets the third constraint. The transparency mask has a minimum feature size of about 15 μm, which is well the below smallest feature in this orthoplanar spring design. All fabrication constraints are thus met, which also fulfills the fourth design requirement. An additional advantage of this design is that it is a very compact system. Two disadvantages include the lack of displacement restraints to prevent the spring from being displaced beyond its intended limits and the need to fabricate a new suspension with each chip.

3.2.2 ABS Plastic Single Suspension

A second suspension design was made of ABS plastic according the parameter values listed in Table 3.2, resulting in a safety factor of 3.64. It uses a single three-legged orthoplanar spring,

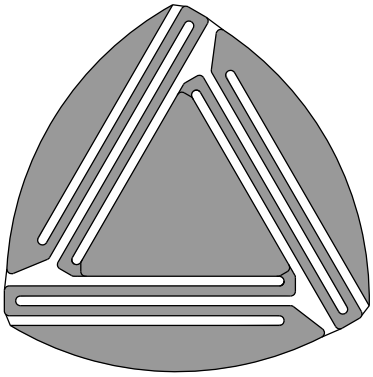

(a) Orthoplanar spring line diagram

(b) Bottom view of suspension

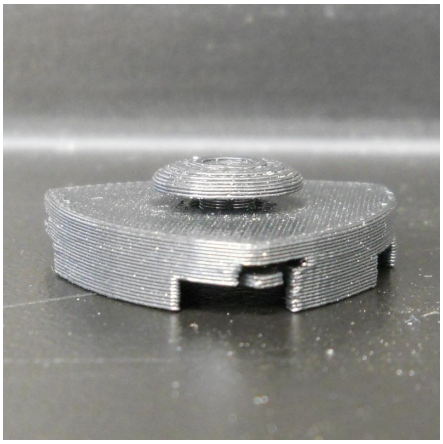

(c) Side view of suspension

Figure 3.3: This reusable suspension made of ABS plastic uses a single three-legged orthoplanar spring.

which again fails to restrain rotations about the horizontal axis (see Figure 3.3). The chip is attached to the platform with double sided tape, meeting the first design constraint and allowing the suspension to be reused. However, it does not incorporate an electrical system for attraction and repulsion, so it does not meet the second requirement. The suspension is smaller than the culture dish, according to constraint three. The smallest dimension of the suspension is equal to the minimum dimension size of 0.77 mm required by the three dimensional printing process used. An additional advantage of the suspension is that it includes displacement restraints to help prevent failure.

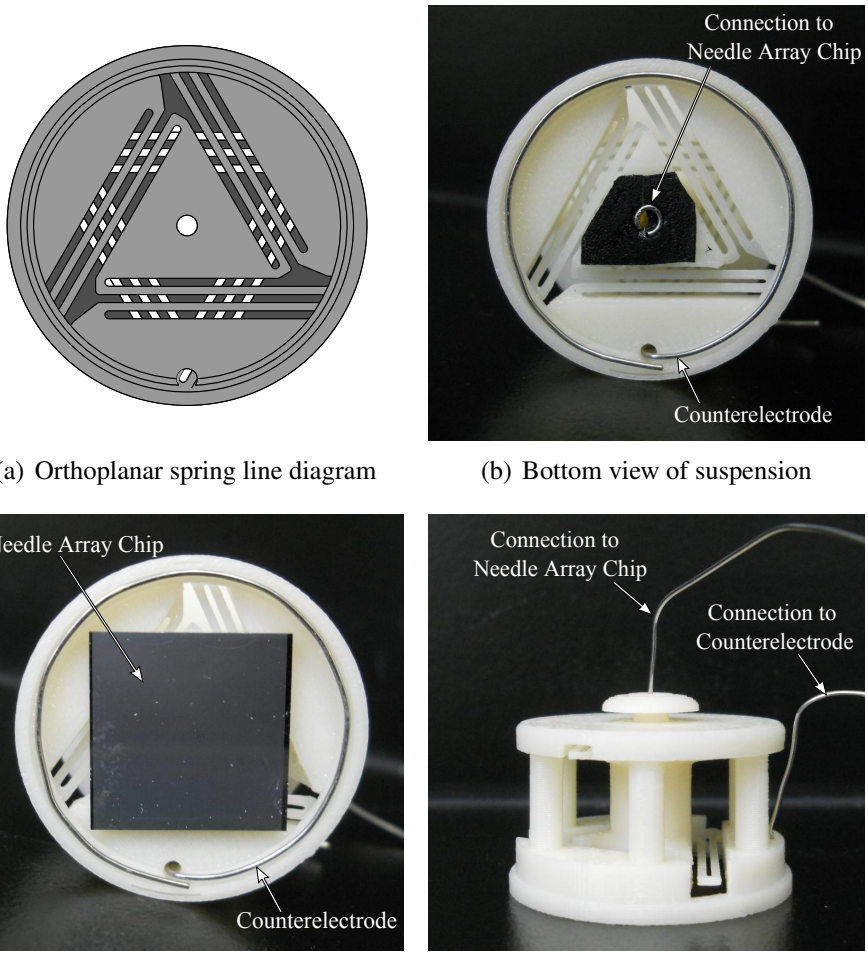

(a) Orthoplanar spring line diagram

(b) Bottom view of suspension

(c) Bottom view of suspension with chip

(d) Side view of suspension

Figure 3.4: This reusable suspension made of ABS plastic uses a second three-legged orthoplanar spring that is offset vertically from the first and rotated 60° for added stability.

3.2.3 ABS Plastic Double Suspension

The third suspension design also uses ABS plastic, is reusable, and follows the same parameter values for the orthoplanar spring that are listed in Table 3.2. It also includes a second orthoplanar spring that has been offset vertically and rotated 60° (see Figure 3.4). This proved effective at restraining rotations about the horizontal axis and more fully met the first design objective. A hole in the platform allows an electrical connection to the chip. Another hole and recess in the base allow a wire to surround the chip as a counter electrode. Stainless steel wire was selected to prevent corrosion in the saline solutions used in the injection process. The chip is attached using double-sided conductive carbon tape. In this way the second design requirement is fully met. The

base of the suspension exactly matches the 34.80 mm diameter of the culture dish and is taller than the 17.4 mm depth. This not only fulfills the third design constraint, but it also further secures the chip against lateral displacement. The minimum dimension of this suspension is also 0.77 mm to meet the fabrication requirements, as specified by design constraint four.

3.3 Conclusion

This chapter specified the design objectives and constraints associated with the injection system. It also described three injection systems, all of which use a compliant orthoplanar spring as a suspension to allow controlled insertion of the needle array into the cell monolayer. The third design included two offset orthoplanar springs that proved effective in restraining all unwanted linear and rotational deflections. Only the third design incorporated a counterelectrode and electrical connections. These were made using stainless steel wire to avoid corrosion. While all three suspensions fit inside the cell culture dish, the third suspension fit the bottom of the dish exactly to further minimize lateral displacements. It was also made to be taller than the dish was deep to allow for easy removal without disturbing the cells. All three suspensions were designed to meet fabrication requirements.

Table 3.1: Design parameters for the silicon orthoplanar suspension.

Parameter	Value
Displacement (δ)	1 mm
Young's modulus (E)	130 GPa
Flexible segment length (L)	14.6 mm
Number of legs (s)	4
Out-of-plane thickness (h)	0.25 mm
In-plane width (b)	0.30 mm
Flexible segment offset (e)	0.40 mm
Ultimate tensile strength (S_{ut})	0.93 GPa
Ultimate compressive strength (S_{uc})	1.2 GPa
C_T	4.56
Safety factor (SF)	2.47

Table 3.2: Design parameters for the ABS plastic suspensions.

Parameter	Value
Displacement (δ)	1.5 mm
Young's modulus (E)	2320 MPa
Flexible segment length (L)	20.58 mm
Number of legs (s)	3
Out-of-plane thickness (h)	0.77 mm
In-plane width (b)	0.80 mm
Flexible segment offset (e)	1.57 mm
Yield strength (S_y)	37 MPa
C_T	4.77
Safety factor (SF)	3.64

CHAPTER 4. TESTING WITH HELA CELLS

Several tests were performed using the needle array nanoinjection system. The injection protocol used is specified in the first section. The effect of injections on the needle array is described in the second section. The following section reports the cell viability resulting from needle insertion only, applied voltage only, and the complete injection process using needle insertion with voltage. The final two sections describe dye uptake from injecting with and without voltage. Zero voltage injections were performed with high concentrations of membrane impermeable dye in the cell media, and the resulting diffusion of dye into the cells shows that the needles are penetrating the cells. Multiple tests were performed using a smaller concentration of dye to compare dye uptake from injections with and without voltage. Because of large variation in the results, these tests do not conclusively show injections with voltage as being more effective. Glass cover slips were placed in the culture dishes to provide more consistent injection conditions. Tests were performed without voltage on glass and produce more consistent results.

4.1 Injection Protocol

This section describes the full protocol used for testing. The injection setup is shown in Figure 4.1. Some steps were modified for specific tests and are described in the appropriate sections.

4.1.1 HeLa 229 Cell Culturing

HeLa 229 cells are cultured in media consisting of Dulbeccos Modified Eagle Medium (DMEM) with fetal bovine serum (FBS) and gentamycin (see Figure 4.2) [19]. The cells are prepared for testing in six-well plates (9.5 cm^2 growing area per well). To ensure that the cells in the testing wells are approximately within the 2 x 2 cm injection area, a wax boundary is drawn in the center of each well. 0.15 or 0.2 mL of media with HeLa cells is placed within the wax

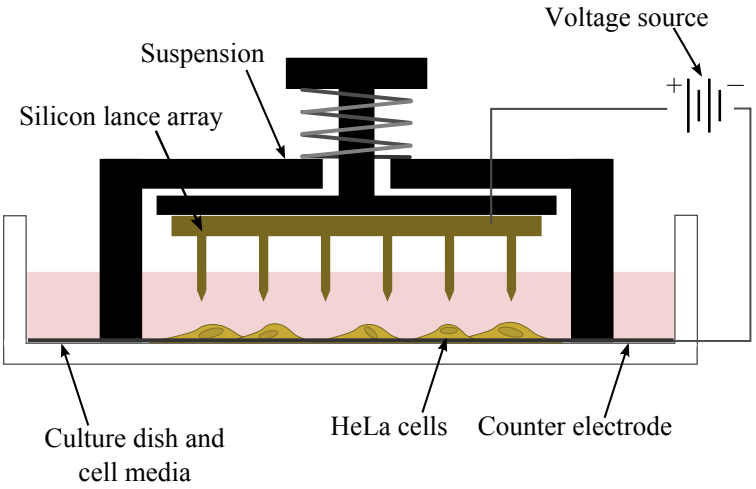

(a) Schematic of the injection system

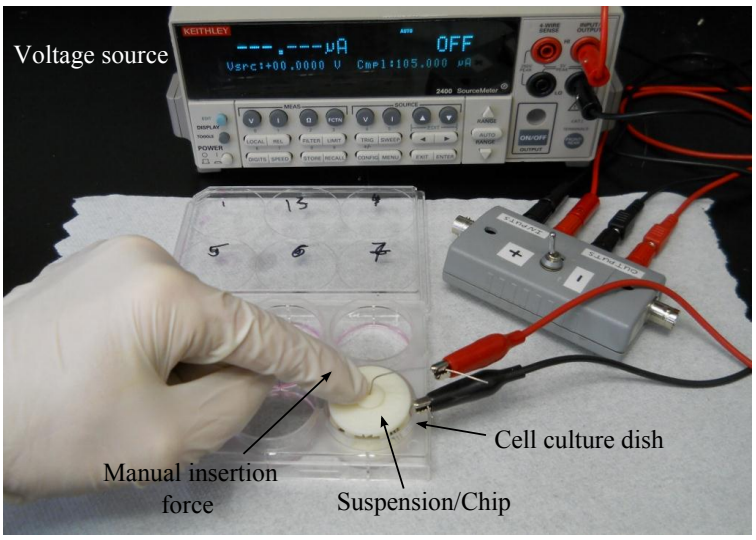

(b) Photograph of the injection setup

Figure 4.1: The suspension and chip are placed in a culture dish with HeLa cells. Voltage is used to attract and repel charged particles, such as a dye or DNA. Manual force is used to insert the needle array into the layer of HeLa cells.

boundary. After one to two hours, the HeLa cells have adhered to the bottom of the culture dish. 2 mL of additional media is added to each well, flooding the bottom of the dish.

4.1.2 Injection

The media is removed from the six wells, and all wells are rinsed with Hanks Balanced Saline Solution (HBSS) to remove dead cells. 1 mL of HBSS is added to each well. The desired

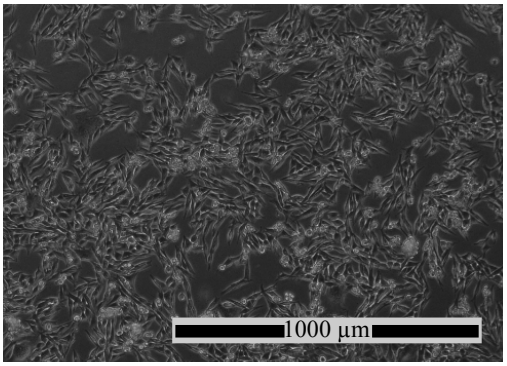

Figure 4.2: This optical micrographs shows a monolayer of HeLa cells in a culture dish.

amount of propidium iodide, a membrane impermeable dye with two positive charges, is added to the wells. A 2 x 2 cm lance array chip is attached to the suspension to allow displacements in the vertical direction. The suspension and chip are lowered into a testing well. A negative voltage is applied between the chip and the counterelectrode for a specified time to attract the dye. A force is applied manually to the suspension for 3 to 5 seconds, pushing the lance array down into the cells, during which time the voltage is made positive to release the dye from the needles. When released, the spring force in the suspension lifts the lance array out of the layer of cells, and the suspension and chip are removed from the well. This is repeated for the other testing wells.

4.1.3 Cell Harvest

After injections, 1 mL of 5x Trypsin is added to each well. The six-well plate is placed in an incubator for 4 to 7 minutes, after which the cells have detached from the bottom of the wells. 1 mL of media is then added to deactivate the Trypsin. The contents of each well are centrifuged for 10 minutes at 2000 rpm. The supernatant is removed, and the pellet of cells is resuspended in the remaining media.

4.2 Needle Array Robustness

Scanning electron micrographs (SEMs) were taken of the lance array chips before and after injections (see Figure 4.3). They show that the vast majority of the lances remained unbroken. It was common for several rows of lances to be broken along one edge of the chips; this was probably

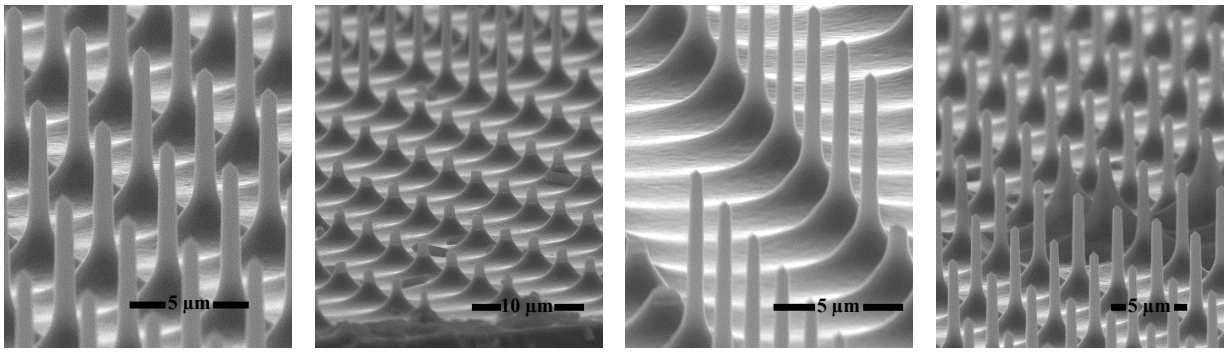

(a) Most needles unbroken (b) Edge needles broken (c) Thin needles broken (d) Cell debris

Figure 4.3: (a) The vast majority of the lances remained unbroken. (b) It was common for several rows of lances to be broken along one edge of the chips. (c) The thinner lances towards the edge of the chip occasionally broke. (c) Some cell debris remained on the chips.

due to one side of the chip meeting the bottom of the well first. The lances toward the edge of the chips were generally thinner than those toward the center, and these thinner lances (usually less than 0.5 μm) occasionally broke. Some cell debris remained on the chips, which may have been from cells that had previously died and for that reason were not firmly attached to the bottom of the well. Most cell debris can be avoided by rinsing the well before testing and by testing with lower cell confluency.

4.3 Cell Viability

Cell viability was determined using one or more of three different viability stains: Trypan blue, propidium iodide, and Sytox® green. Trypan blue allows the analysis of cell viability visually, but it is toxic to cells over time, making the results less stable [32]. For this reason, the two additional stains were used to verify viability results. When used, Trypan blue was added in a 1:1 ratio. A portion of this solution was placed on a slide, and the dead and living cells were counted visually. Propidium iodide was added after cell harvest if being used only as a viability stain, otherwise, it was added before injecting. Cells were assessed using flow cytometry. Sytox® green was added after cell harvest. The cells were incubated for about 20 minutes at room temperature before being assessed with flow cytometry.

Propidium iodide (0.5 mg/mL) was used both as the dye being injected and as a viability stain. This dye has a double positive charge and a molecular weight of 668.4 g/mol. Cells express-

ing moderate levels of propidium iodide were considered successfully injected. Cells expressing high levels of propidium iodide were considered dead [33]. These expression levels were determined based on negative and positive control groups. The positive control group was created by permeabilizing cells for 10 minutes in chilled acetone at below freezing temperatures [34]. In order to verify the accuracy of this method of determining cell viability, Sytox® green was also used in some tests. They produced very similar viability results (see Table 4.1).

4.3.1 Needle Insertion Only

These tests were performed using the given testing protocol but without using any voltage. All three viability stains were used in different tests to verify accuracy. Control groups that were not injected were also kept. All three methods reported very similar cell viability results of around 97%, as shown in Table 4.1.

4.3.2 Voltage Only

The testing protocol was modified to include the application of voltage without needle insertion. 1, 2, 4, 5, and 10 volts were applied to the chip in separate wells. Propidium iodide was used as the viability stain. The viability results are shown in Table 4.2. Voltage does not seem to cause a significant decrease in cell viability.

Table 4.1: Viability results from testing without voltage used three viability stains.

Viability Stain	Tested			Control		
	Living Cells	Total Assessed	Viability	Living Cells	Total Assessed	Viability
Trypan blue	4288	4428	96.9%	6040	6115	98.8%
Propidium iodide	71489	72815	98.2%	43348	43475	99.7%
Sytox® green	32234	33270	96.9%	42216	42447	99.5%

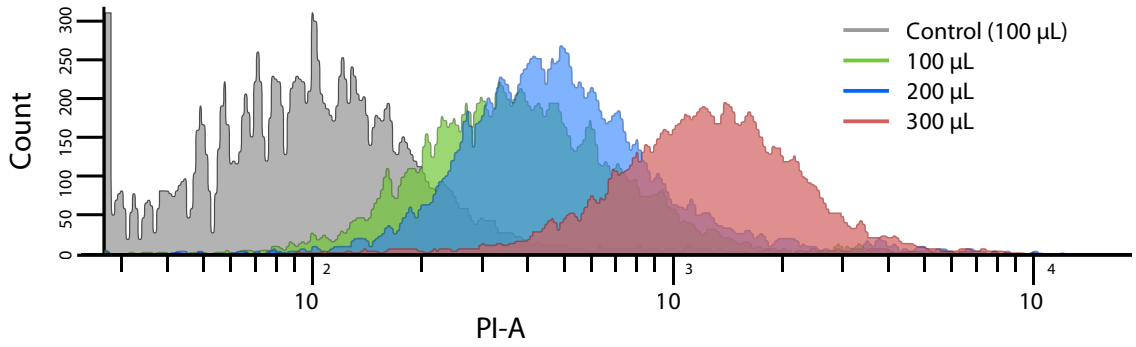

Figure 4.4: These results from flow cytometry show that the cells receive the dye through injection without voltage when there is a high concentration of dye in the media.

4.3.3 Needle Insertion with Voltage

The viability resulting from the full testing protocol was measured using propidium iodide. The high viability shows that using the nanoinjection process with the needle array has little effect on cell death, even with voltages up to 30 V (see Table 4.3).

4.4 Injection without Voltage

Injections done without voltage in a high concentration of dye showed that the needles pierce the cell membranes. Multiple dishes of HeLa cells were prepared according to the protocol. One control well received 100 μL of propidium iodide and was not injected. Three additional wells received 100, 200, and 300 μL of propidium iodide, respectively, and were injected. The cells were analyzed using flow cytometry. The control well shows the background fluorescence due to 100

Table 4.2: Viability results from applying voltage without needle insertion using propidium iodide.

Applied Voltage	Living Cells	Total Assessed	Viability
0	26240	26342	99.6%
-1	24635	24992	98.6%
-2	22829	23487	97.2%
-3	16283	16970	96.0%
-4	8464	8548	99.0%
-5	8520	8561	99.5%
-10	6088	6141	99.1%

μL of propidium iodide in the well. The plots in Figure 4.4 show the uptake of dye into the cells due to the diffusion through the holes made in the cell membrane by the needles. Table 4.4 reports the percentage of cells in each well that express fluorescence above a chosen value.The large gap between the 100 μL control group and the 100 μL test group verify penetration of the cells by the needles. It is also seen that the higher concentrations of dye result in higher expression, although it should be noted that they may have higher levels of background fluorescence than shown by the 100 μL control.

4.5 Injection with Voltage

The full injection process was performed using 20 μL of propidium iodide per well, resulting in a dye concentration of 0.01 mg/mL. Testing was done using six-well culture plates. The dye uptake percentages shown in Table 4.5 were divided into two groups: voltage injections and zero voltage injections. These percentages were compared on a log scale using a t-test. The resulting 2-tailed p-value of 0.6844 showed that there was no significant difference between injecting with and without voltage using the specified protocol.

However, the well in which each test was performed was tracked to report any correlation between dye uptake and the well, as shown in Table 4.5. The dye uptake percentages of each well were compared to the dye uptake of the other five wells on a log scale using a t-test. The 2-tailed p-values are reported in the table. They show that there is a statistically significant trend concerning well two and well four. Well two consistently yielded low dye uptake (below 5%), and well four consistently yielded higher dye uptake (above 25%). This implies that some of the variation is due to the bottom surface of the wells.

Table 4.3: Viability results from applying voltage with needle insertion using propidium iodide.

Applied Voltage	Living Cells	Total Assessed	Viability
-1	9280	9344	99.3%
-10	89131	90927	98.0%
-20	50863	51769	98.2%
-30	3524	3551	99.2%

Glass cover slips were placed in the bottom of the wells before cell culture to provide a more uniform injection surface. Four six-well plates were prepared in this way and injected without voltage using three different chips. 20 μL of dye was again used. The dye uptake results are shown in Table 4.6. These percentages were also analyzed for trends using the same method, and no statistically significant trend was found. Therefore, placing glass cover slips in the wells was significant in removing the trend associated with wells two and four. Future injections with voltage should be performed using this protocol.

The standard deviations of the dye uptake percentages were calculated for each round of testing. The standard deviations from the eight tests without glass were compared on a log scale using a t-test to those from the three tests done with glass cover slips. The resulting 2-tail p-value of 0.2019 does not conclusively show that testing on glass cover slips reduces variation in testing, but it is suggestive of that fact.

4.6 Conclusion

Multiple tests were performed and reported in this chapter. The injection protocol used was described. The tests show that the needle array used is sufficiently robust for the injection process. All cell viability results were greater than or equal to 96.0%, and the total viability from the complete injection process was 98.2%. Zero volt injections using large concentrations of membrane impermeable dye resulted in the diffusion of dye into the cells. This proved that the needles are penetrating the cells. However, tests comparing dye uptake from injecting with and without voltage showed no significant difference between the two processes. Trends were found relating to which well was used during the injection. Further tests done without voltage on glass

Table 4.4: Cell fluorescence results from injecting without voltage using three different concentrations of dye.

Test	Dye Concentration (mg/mL)	Fluorescing Cells	Total Assessed	Percentage
Control (100 μL)	0.05	557	9500	5.9%
100 μL	0.05	5517	8184	67.4%
200 μL	0.10	7394	8918	82.9%
300 μL	0.15	6686	6827	97.9%

cover slips placed in the culture wells removed those trends. Future tests with voltage should also be done on glass cover slips.

Table 4.5: These cell fluorescence results are from injecting with and without voltage on the original culture dish floor and are arranged by well number. 20 μL of dye was used, resulting in a dye concentration of 0.01 mg/mL. The p-values that are marked with an asterisk ($*$) report a significant difference between the uptake of that well and the remaining five wells.

	Dye Uptake (Voltage)					
Test	Well 1	Well 2	Well 3	Well 4	Well 5	Well 6
1	—	—	13.8% (1 V)	31.4% (10 V)	10.2% (0 V)	14.2% (1 V)
2	26.7% (0 V)	3.2% (0 V)	50.4% (10 V)	40.9% (10 V)	—	—
3	—	4.6% (10 V)	9.5% (10 V)	25.1% (10 V)	10.7% (10 V)	14.4% (10 V)
4	—	4.8% (0 V)	10.4% (0 V)	31.1% (0 V)	7.3% (0 V)	15.0% (0 V)
5	14.8% (10 V)	3.6% (10 V)	—	29.1% (0 V)	15.5% (10 V)	9.8% (10 V)
6	15.6% (10 V)	—	23.1% (20 V)	—	11.1% (30 V)	—
7	9% (0 V)	—	10.1% (20 V)	—	14.1% (20 V)	15.8% (20 V)
8	44.9% (0 V)	—	39.4% (20 V)	—	10.1% (20 V)	9.6% (20 V)
Mean	22.2%	4.05%	22.4%	31.5%	11.3%	13.1%
2-tailed p-value	0.0597	$< .0001^*$	0.0667	$< .0001^*$	0.1921	0.7730

Table 4.6: These cell fluorescence results are from injecting without voltage on glass cover slips and are arranged by well number.

	Needle	Dye Uptake					
Test	Diameter	Well 1	Well 2	Well 3	Well 4	Well 5	Well 6
1	1.0 μm	—	9.1%	12.0%	12.6%	13.2%	17.2%
2	1.25 μm	3.8%	9.2%	12.6%	—	2.5%	3.5%
3	1.4 μm	—	40.3%	31.9%	40.8%	61.1%	52.7%
		—	48.4%	50.0%	61.5%	41.9%	43.7%

CHAPTER 5. CONCLUSION

5.1 Contributions

The following list summarizes the contributions made by the research presented in this thesis.

- Developed a process to fabricate needle arrays that are able to penetrate cells without causing significant cell death.
- Designed a system for performing injections.
- Created a protocol for the lance array injection system and performed testing using a dye.

While much work has been done to create fabrication methods for microneedles, most of the needles produced are on the order of 100 μm tall. These fabrication methods have been adapted to the smaller scale required to inject individual somatic cells. The process is built around three DRIE steps (unpassivated, passivated, and unpassivated again) to create needles with a constant diameter shaft that terminate in a sharp point. Additional steps remove the passivation layer and photoresist mask. This process has successfully produced millions of needles with an average diameter of about 1 μm, average height of 8 μm, and 10 μm center-to-center spacing.

The system for performing injections centers around a plastic suspension that uses two orthoplanar springs to allow vertical displacements while minimizing all other linear and rotational displacements. It includes one electrical connection to the area where the silicon needle array chip is attached. There is another electrical connection to the stainless steel ring that surrounds the chip and acts as the counterelectrode. These two electrical leads connect to a voltage source and allow the nanoinjection process to be used.

The injection protocol describes the preparation of the cells, the actual injection procedure, and cell harvesting for analysis. The needle arrays were examined after testing, and the vast majority of needles in the arrays proved to be undamaged. The injection protocol was followed with

variations to report cell viability due to needle insertion, voltage, and a combination of the two. The average cell viability for the full injection protocol was 98.2%. Zero volt cell injections with a high concentration of dye verified that the needles penetrate the cells. Dye uptake under these circumstances is the result of diffusion. Preliminary tests to inject dye using the complete protocol resulted in high variability. Modifying the protocol to include glass cover slips on the bottom of each well led to more uniform results within each test.

5.2 Future Work

Possible testing in the future includes injecting with voltage on the glass cover slips. The results without voltage were more consistent with the glass cover slips to provide a more uniform injection surface. Therefore, any difference between results from testing with and without voltage would be more clear when testing on glass.

Mathematical modeling showed that using a conductive plate directly underneath the cells was more effective than the ring electrode presented in this thesis. The glass cover slips could be replaced by electrically conductive plates to act as the counterelectrode. The current suspension would still work in this situation because the ring electrode would come in contact with the plate electrode. One possible issue is how well the cells to adhere each material used. If the cells do not adhere well, they might be pulled off the counterelectrode when the needle array is removed. However, it may be possible to coat the counterelectrode with a material that would allow improved cell adhesion.

DNA should be used to perform the injections in addition to the dye. DNA has already been shown to work with the nanoinjection process using the single-cell nanoinjector described in the introduction. This would remove one unknown variable from the system if performing nanoinjection with the dye is not producing significant results. Also, the ability to insert DNA into cells is of greater value than injecting a dye.

The geometry of the needles themselves may have an important impact on the injection process. Studies may be done changing needle diameter or length. For example, a larger diameter would result in a larger surface area to which particle could be attracted. However, the larger cross-sectional area may have a negative impact on cell viability. Different mask shapes, such as

triangles, could be used to increase the surface area while maintaining the same cross-sectional area.

REFERENCES

[1] Luo, D., and Saltzman, W. M., 2000. "Synthetic DNA delivery systems." *Nature Biotechnology,* **18**, pp. 33–37.

[2] Mehier-Humbert, S., and Guy, R. H., 2005. "Physical methods for gene transfer: Improving the kinetics of gene delivery into cells." *Advanced Drug Delivery Reviews,* **57**, pp. 733–753.

[3] Aten, Q. T., Jensen, B. D., and Burnett, S. H., 2008. "Testing of a pumpless MEMS microinjection needle employing electrostatic attraction and repulsion of DNA." In *2008 Proceedings of the ASME International Design Engineering Technical Conferences and Computers and Information in Engineering Conference, DETC2008*.

[4] Aten, Q. T., 2008. "Design and testing of a pumpless microelectromechanical system nanoinjector." Master's thesis, Brigham Young University.

[5] Aten, Q. T., Jensen, B. D., Burnett, S. H., and Howell, L. L., 2011. "Electrostatic accumulation and release of DNA using a micromachined lance." *Journal of Microelectromechanical Systems,* **20**(6), December, pp. 1449–1461.

[6] Aten, Q. T., Jensen, B. D., Burnett, S. H., and Howell, L. L., In Review 2011. "A self-reconfiguring metamorphic nanoinjector for injection into mouse zygotes." *Journal of Microelectromechanical Systems*.

[7] David, R. A., Jensen, B. D., Black, J. L., Burnett, S. H., and Howell, L. L., 2011. "Study of design parameters affecting the motion of DNA for nanoinjection." *Journal of Micromechanics and Microengineering,* **22**(5), pp. 1–10.

[8] Fernelius, M. H., Toone, N. C., Jensen, B. D., Burnett, S. H., and Howell, L. L., 2011. "Preliminary studies of stand-alone lance concepts for nanoinjection of DNA." In *ASME 2011 International Mechanical Engineering Congress & Exposition*.

[9] Aten, Q., Jensen, B., Tamowski, S., Wilson, A., Howell, L., and Burnett, S., 2012. "Nanoinjection: pronuclear DNA delivery using a charged lance." *Transgenic Research*, pp. 1–12 10.1007/s11248-012-9610-6.

[10] Chun, K., Hashiguchi, G., Toshiyoshi, H., and Fujita, H., 1999. "Fabrication of array of hollow microcapillaries used for injection of genetic materials into animal/plant cells." *Japanese Journal of Applied Physics,* **38**, pp. L279–L281.

[11] Kaushik, S., Hord, A. H., Denson, D. D., McAllister, D. V., Smitra, S., Allen, M. G., and Prausnitz, M. R., 2001. "Lack of pain associated with microfabricated microneedles." *Anesthesia and Analgesia,* **92**, pp. 502–504.

[12] Hanein, Y., Schabmueller, C. G. J., Holman, G., Lucke, P., Denton, D. D., and Bohringer, K. F., 2003. "High-aspect ratio submicrometer needles for intracellular applications." *Journal of Micromechanics and Microengineering,* **13**, pp. S91–S95.

[13] Prausnitz, M. R., 2004. "Microneedles for transdermal drug delivery." *Advanced Drug Delivery Reviews,* **56**, pp. 581–587.

[14] Wilke, N., Hibert, C., OBrien, J., and Morrissey, A., 2005. "Silicon microneedle electrode array with temperature monitoring for electroporation." *Sensors and Actuators,* **123-124**, pp. 319–325.

[15] Diehl, M. S., 2007. "Design and fabrication of out-of-plane silicon microneedles with integrated hydrophobic microchannels." Master's thesis, Brigham Young University.

[16] McAllister, D. V., Wang, P. M., Davis, S. P., Park, J.-H., Canatella, P. J., Allen, M. G., and Prausnitz, M. R., 2003. "Microfabricated needles for transdermal delivery of macromolecules and nanoparticles: Fabrication methods and transport studies." *PNAS,* **100**, pp. 13755–13760.

[17] Choi, S.-O., Kim, Y. C., Park, J.-H., Hutcheson, J., Gill, H. S., Yoon, Y.-K., Prausnitz, M. R., and Allen, M. G., 2010. "An electrically active microneedle array for electroporation." *Biomedical Microdevices,* **12**(2), pp. 263–273.

[18] Gassend, B. L. P., Velsquez-Garca, L. F., and Akinwande, A. I., 2010. "Design and fabrication of DRIE-patterned complex needlelike silicon structures." *Journal of Microelectromechanical Systems,* **19**(3), June, pp. 589–598.

[19] Freshney, R. I., 2010. *Culture of animal cells: a manual of basic technique and specialized applications*. Wiley-Blackwell.

[20] Lue, N., Choi, W., Popescu, G., Yaqoob, Z., Badizadegan, K., Dasari, R. R., and Feld, M. S., 2009. "Live cell refractometry using hilbert phase microscopy and confocal reflectance microscopy." *Journal of Physical Chemistry A,* **113**(47), November, pp. 13327–133330.

[21] Ng, C., Wong, M., Lam, R., Ho, J., and Yu, K., 2011. "Fabrication of pseudo three-dimensional PADC cell culture substrates for dosimetric studies." *Radiation Measurements,* **46**, pp. 1790–1794.

[22] Laermer, F., and Urban, A., 2003. "Challenges, developments and applications of silicon deep reactive ion etching." *Microelectronic Engineering,* **67-68**, pp. 349–355.

[23] Jansen, H., de Boer, M., Legtenberg, R., and Elwenspoek, M., 1995. "The black silicon method: a universal method for determining the parameter setting of a fluorine-based reactive ion etcher in deep silicon trench etching with profile control." *Journal of Micromechanics and Microengineering,* **5**, pp. 115–120.

[24] Jansen, H., de Boer, M., Otter, B., and Elwenspoek, M., 1995. "The black silicon method IV: The fabrication of three-dimensional structures in silicon with high aspect ratios for scanning probe microscopy and other applications." In *Proceedings of MEMS '95, 8th IEEE International Workshop Micro Electromechanical System*, pp. 88–93.

[25] Li, R., Lamy, Y., Besling, W. F. A., Roozeboom, F., and Sarro, P. M., 2008. "Continuous deep reactive ion etching of tapered via holes for three-dimensional integration." *Journal of Microm,* **18**, pp. 1–8.

[26] Norton, R. L., 2006. *Machine Design: An Integrated Approach*., 3 ed. Pearson Education, Inc.

[27] Liu, C., 2006. *Foundations of MEMS*. Pearson Education, Inc.

[28] Obataya, I., Nakamura, C., Han, S. W., Nakamura, N., and Miyake, J., 2005. "Mechanical sensing of the penetration of various nanoneedles into a living cell using atomic force microscopy." *Bionsensors and Bioelectronics,* **20**, pp. 1652–1655.

[29] Howell, L. L., 2001. *Compliant Mechanisms*. John Wiley & Sons, Inc.

[30] Parise, J. J., Howell, L. L., and Magleby, S. P., 2001. "Ortho-planar linear-motion springs." *Mechanism and Machine Theory,* **36**, pp. 1281–11299.

[31] Namazu, T., Isono, Y., and Tanaka, T., 2000. "Evaluation of size effect on mechanical properties of single crystal silicon by nanoscale bending test using AFM." *Journal of Mi,* **9**(4), December, pp. 450–459.

[32] Mascotti, K., McCullough, J., and Burger, S., 2000. "HPC viability measurement: trypan blue versus acridine orange and propidium iodide." *Transfusion,* **40**, pp. 693–696.

[33] Djuzenova, C. S., Zimmermann, U., Frank, H., Sukhorukov, V. L., Richter, E., and Fuhr, G., 1996. "Effect of medium conductivity and composition on the uptake of propidium iodide into electropermeabilized myeloma cells." *Biochimica et Biophysica Acta,* **1284**, pp. 143–152.

[34] Jamur, M. C., and Oliver, C., 2010. "Permeabilization of cell membranes." *Methods in Molecular Biology,* **588**, pp. 63–66.

APPENDIX A. EQUIPMENT SETTINGS FOR THE DRIE STEPS IN THE NEEDLE FABRICATION

The deep reactive ion etching (DRIE) was performed using Surface Technology Systems (STS) Multiplex ICP Etch equipment. The following tables show the settings used in the unpassivated DRIE step (Table A.1), the passivated DRIE (Bosch) step (Table A.2), and the oxygen plasma step (Table A.3).

Table A.1: The settings used in the unpassivated DRIE step using STS Multiplex ICP Etch equipment.

Setting	Value
Gas Flow	50 sccm SF_6
Coil Power	700 W
Platen Power	15 W
Pressure	15 mTorr

Table A.2: The settings used in the passivated DRIE (Bosch) step using STS Multiplex ICP Etch equipment.

Setting	Value
Etch Step	5.0 sec
Passivation Step	5.0 sec
First Step	Passivation
Etch Gas Flow	130 sccm SF_6 + 13 sccm O_2
Passivation Gas Flow	85 sccm C_4F_8
Coil Power	600 W
Platen Power	15 W

Table A.3: The settings used in the oxygen plasma step using STS Multiplex ICP Etch equipment.

Setting	Value
SF_6 Gas Flow	50 sccm
Coil Power	700 W
Platen Power	15 W
Pressure	15 mTorr